Ultrafast spinning twisted ribbons of confined electric fields

Bauer, Thomas; Khonina, Svetlana N.; Golub, Ilya; Leuchs, Gerd; Banzer, Peter

DOI
10.1364/OPTICA.392772

Publication date
2020

Document Version
Final published version

Published in
Optica

optica

Ultrafast spinning twisted ribbons of confined electric fields

Thomas Bauer,[1] Svetlana N. Khonina,[2,3] Ilya Golub,[4,7] Gerd Leuchs,[5,6] and Peter Banzer[5,6,*]

[1]Kavli Institute of Nanoscience Delft, Delft University of Technology, Lorentzweg 1, Delft 2628 CJ, The Netherlands
[2]IPSI RAS–Branch of the FSRC "Crystallography and Photonics" RAS, 151 Molodogvardeiskaya Str., Samara 443001, Russia
[3]Samara National Research University, 34 Moskovskoye Shosse, Samara 443086, Russia
[4]School of Advanced Technology, Algonquin College, Ottawa, Ontario K2G 1V8, Canada
[5]Max Planck Institute for the Science of Light, Staudtstr. 2, D-91058 Erlangen, Germany
[6]Institute of Optics, Information and Photonics, Friedrich-Alexander-University Erlangen-Nuremberg, Staudtstr. 7/B2, D-91058 Erlangen, Germany
[7]e-mail: ilya.golub@rogers.com
*Corresponding author: peter.banzer@mpl.mpg.de

Received 13 March 2020; revised 6 July 2020; accepted 9 August 2020 (Doc. ID 392772); published 21 September 2020

Topological properties of light attract tremendous attention in the optics communities and beyond. For instance, light beams gain robustness against certain deformations when carrying topological features, enabling intriguing applications. We report on the observation of a topological structure contained in an optical beam, i.e., a twisted ribbon formed by the electric field vector *per se*, in stark contrast to recently reported studies dealing with topological structures based on the distribution of the time averaged polarization ellipse. Moreover, our ribbons are spinning in time at a frequency given by the optical frequency divided by the total angular momentum of the incoming beam. The number of full twists of the ribbon is equal to the orbital angular momentum of the longitudinal component of the employed light beam upon tight focusing, which is a direct consequence of spin-to-orbit coupling. We study this angular-momentum-transfer-assisted generation of the twisted ribbon structures theoretically and experimentally for tightly focused circularly polarized beams of different vorticity, paving the way to tailored topologically robust excitations of novel coherent light–matter states.

https://doi.org/10.1364/OPTICA.392772

The topological structure of light beams is enriched by spin–orbit interactions (SOI) or the interplay of spin angular momentum (SAM), associated with the polarization of light, and the orbital angular momentum (OAM), which is related to the spatial structure of the beam's wavefront [1,2]. While complex topological structures such as optical vortices, polarization knots [3,4], and optical polarization Möbius strips [5,6] were extensively studied and even observed experimentally [3,4,7–10], surprisingly, the experimental observation of an optical twisted ribbon was investigated less actively and reported only very recently [11]. This is despite the fact that an optical ribbon is a ubiquitous structure [12]. It is important to note here that polarization topological structures reported so far have solely been discussed in the context of the polarization ellipse and its major and minor semiaxes [5–8,11,12] or higher-order Lissajous figures [13,14]. In the present study, it is the electric field vector itself, which twists and turns to form a ribbon. Additionally, quite elaborate schemes including interference of several beams or the focusing of multiple co-propagating modes are often required to observe topologies such as optical polarization Möbius strips or ribbons [7,10,11]. In the present work, we show that focusing a circularly polarized light beam with or even without a central phase vortex generates a twisted ribbon of the focal electric field *per se,* spinning in time around the optical axis. Importantly, our optical ribbon can be a "pure" or "true" ribbon in the sense that it manifests itself around a point of zero field intensity and exists by itself while not being accompanied/surrounded by other topological structures. The number of full ribbon twists corresponds to the total angular momentum (AM) in accordance with the index theorem (and equal to the OAM of the longitudinal component of the focused beam) [15]. The theoretical predictions are fully corroborated by experimental results recorded utilizing a nano-interferometric amplitude and phase reconstruction technique [16].

In order to prove the proposed concept of optical twisted ribbons in the time-instantaneous electromagnetic field, we study topological structures created by tight focusing of fundamental Gaussian and first-order Laguerre–Gaussian beams resulting in electric (and magnetic) field ribbons of low twist numbers. For comparison with the full-field experimental data retrieved for the aforementioned tightly focused light beams, we use theoretical data calculated based on vectorial diffraction theory [17]. However, we start our discussion by representing the general structure of highly confined light beams via an approximate analytical model, which will allow us to retrieve a fundamental connection between the AM of the input beam and the twist number of the resulting field ribbons. In this model, we use at the input a narrow ring aperture (see also [18,19]), simplifying the integral equations of vectorial diffraction theory to analytic expressions. For the limiting case of

NA → 1, one obtains the field components of a circularly polarized annular beam with azimuthal index m in a cylindrical [20] as well as Cartesian basis [19],

$$\boldsymbol{E}_m^{\mathrm{circ}} \pm (\rho, \varphi, z) \approx C e^{i(m\pm1)\varphi} A_\theta(z) \times \begin{bmatrix} J_m(k\rho) + J_{m\pm2}(k\rho) \\ \pm i\{J_m(k\rho) - J_{m\pm2}(k\rho)\} \\ \mp 2i J_{m\pm1}(k\rho) \end{bmatrix}_{\rho,\varphi,z}$$

$$= C A_\theta(z) \times \begin{bmatrix} e^{im\varphi} J_m(k\rho) + e^{i(m\pm2)\varphi} J_{m\pm2}(k\rho) \\ \pm i\left\{e^{im\varphi} J_m(k\rho) - e^{i(m\pm2)\varphi} J_{m\pm2}(k\rho)\right\} \\ \mp 2i e^{i(m\pm1)\varphi} J_{m\pm1}(k\rho) \end{bmatrix}_{x,y,z}. \quad (1)$$

Here «±» represents either clockwise (cw; +) or counterclockwise (ccw; −) circular polarization, with the direction of rotation defined as seen by an observer toward whom the wave is propagating. m is the azimuthal order or vorticity of the initial light field. A corresponds to the resulting amplitude function imprinted by the geometry of the ring aperture at a focusing angle of θ, and J_m is the mth order Bessel function of first kind, with k the wavenumber of the incident light, $C = -kf\frac{i^{m+1}}{2\sqrt{2}}$ a prefactor with f the focal length of the focusing lens, and (ρ, φ, z) the employed cylindrical coordinates. The time dependence $\exp[i\omega t]$ is here implicit. The main features contained in the above equation hold even for a finite annular aperture of 20° angular width [21]. Consequently, it is justified to use Eq. (1) for our analysis. The main difference to the experimental realization is the appearance of noteworthy sidelobes for the annular aperture case, as known from Bessel-like light fields [22,23]. The SOI-induced transformation of the SAM, or «±» circular polarization, to OAM is expressed in an increase/decrease of the vorticity of the longitudinal, i.e., z component by 1 [24]. More importantly, we see that the relative phase change of this component upon a full 360° rotation around the optical axis (2π change in the azimuthal angle φ) of $2\pi(m \pm 1)$, together with the behavior of the transverse components (which are phase-shifted by $\frac{\pi}{2}$ relative to each other) determine the number of full twists of the topological structure (ribbon) formed by the electric (or magnetic) field vector for a snapshot in time. This statement will also be proven numerically and experimentally below. Also note that for cw, or "+" circular polarization, and $m \neq [-2, 0]$, the intensity in the center of the pattern described by Bessel functions with order 1 or higher is zero, rendering our topological structure a "pure" or "true" one for these cases. A similar situation is achieved for "−" or ccw circular polarization and $m \neq [0, 2]$.

Next, we discuss the time evolution of the aforementioned ribbon structure. The components of the electric field in cylindrical coordinates [see Eq. (1)] have their azimuthal coordinate dependence solely given by the common phase factor $\exp[i(m \pm 1)\varphi - i\omega t]$. The temporal evolution of the field is thus uniquely linked to an azimuthal coordinate change by $\frac{d\varphi}{dt} = \frac{\omega}{m\pm1}$. Consequently, the topological structure of the instantaneous electric field vector generated upon tight focusing rotates on a circular trace in the focal plane at a $\frac{1}{m\pm1}$ fraction of the optical frequency [25], or inversely proportional to the total AM of the full field, which is equal to $m \pm 1$.

To demonstrate experimentally the appearance of twisted ribbons in the time-instantaneous electric field distribution, we use the experimental setup shown in Fig. 1, which consists of a homebuilt confocal-like microscope [7,16]. The chosen near-field probe is a single gold nanosphere with a diameter of approximately 80 nm (see scanning electron micrograph in Fig. 1) that is immobilized on a glass substrate. This probe can be precisely scanned through the investigated field distribution using a piezo stage, resulting in scattering of the local electric field at the point of the probe. An oil-immersion microscope objective (NA = 1.3) is collecting the forward-scattered and transmitted light from the substrate side, leading to the angularly resolved detection of their interference by imaging the back focal plane of the microscope objective onto a CCD camera. This Fourier-microscopy-based interference approach is equivalent to observing the scattering process from various directions. Thus, it allows for retrieval of the relative phase information between all three electric field components in the fully vectorial distribution under study from the far field. This technique, labeled Mie-scattering nano-interferometry [16], was proven to achieve deep sub-wavelength spatial resolution in the experimental study of vectorial focal fields and enabled the experimental verification of optical polarization Möbius strips and twisted ribbons in the distribution of the polarization ellipse (major axis) resulting from tailored light fields [7,8,11]. Details regarding this technique are discussed in [16].

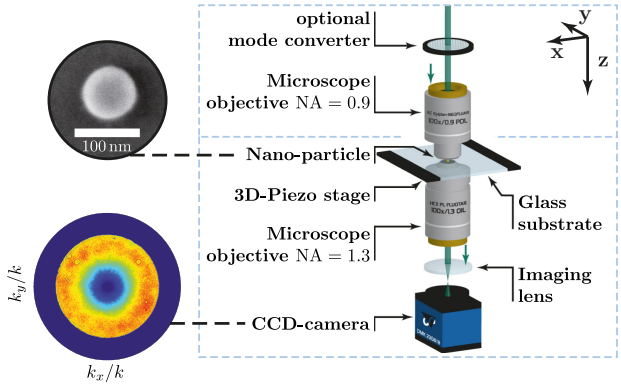

Fig. 1. Sketch of the experimental setup employed to reconstruct the full vectorial focal field distribution of the tightly focused Laguerre–Gaussian and Gaussian beams. The insets show an SEM image of the gold nano-probe, as well as a resulting Fourier-space image of the transmitted and forward-scattered light through the underlying glass substrate—shown for a circularly polarized Laguerre–Gaussian input beam $\mathrm{LG}_1^{\mathrm{circ}+}$—used to reconstruct the full vectorial light field.

From the full amplitude and phase information of the complex vectorial light field reconstructed within the plane of observation, we also retrieve information about the temporal evolution of the field and, thus, the rotation behavior of this topological structure during an optical cycle. Given the common time-dependent phase factor of $\exp[-i\omega t]$ for a harmonically oscillating field, the instantaneous vectorial electric field distribution can be inferred at every time step within the optical cycle by a global phase shift of $\Delta\varphi = \omega\Delta t$.

In contrast to the analytical considerations discussed above, the highly confined focal field distribution containing a twisted ribbon in its time-instantaneous electric field vector is experimentally generated by focusing a circularly polarized Laguerre–Gaussian beam of order m with the full aperture of a microscope objective with an NA of 0.9 (no annular aperture). As stated, this affects only the strength of the sidelobes in the focal field distribution but not the comprised topological structure, while simplifying

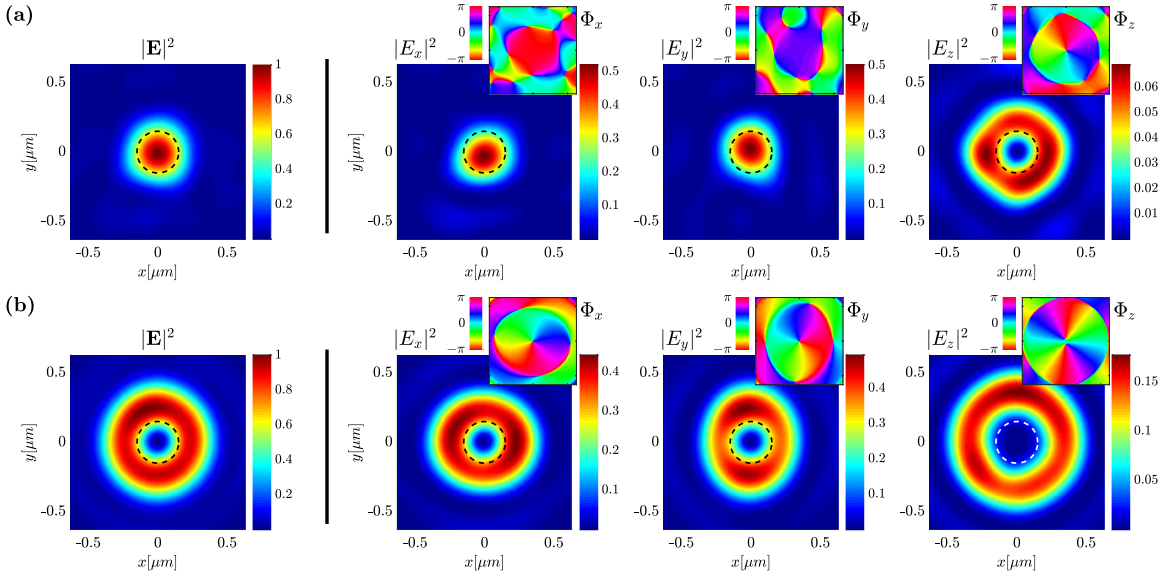

Fig. 2. Experimentally reconstructed electric energy density distribution and its 3D vector components in the focal plane of a tightly focused circularly polarized Laguerre–Gaussian beam of (a) $\mathbf{LG_0^{circ-}}$ and (b) $\mathbf{LG_1^{circ+}}$, respectively. The relative phase distribution of each of the field components is shown as an inset above the respective energy density distribution. Note the zero intensity in the beam center in (b), caused by the presence of phase vortices with $m \geq 1$ in all field components independent of the chosen coordinate basis. The dashed black (or white) circles correspond to the trace chosen to visualize the twisted ribbon structures in Figs. 3 and 4.

the experimental setting. The input beam for $m \neq 0$ is generated by transmitting a circularly polarized Gaussian beam through an optimally tuned $\boldsymbol{q}$-plate [26] of order $q = \frac{m}{2}$. The resulting field with an on-axis phase vortex of charge m and circular polarization of opposite handedness is filtered spatially with a pinhole to obtain the lowest radial order of the created Laguerre–Gaussian modes [27] before being focused by the objective.

For the experimental reconstruction, we scan the nano-probe across the highly confined focal field and apply the reconstruction algorithm detailed in [16] to the collected far-field intensity information. As a result, we retrieve the experimentally reconstructed focal electric energy density and phase distributions shown in Figs. 2(a) and 2(b) for two different input light beams $\mathrm{LG}_0^{\mathrm{circ}-}$ and $\mathrm{LG}_1^{\mathrm{circ}+}$, respectively. The excitation wavelength in this case was chosen as $\lambda = 530$ nm, with the nano-probe exhibiting an experimentally determined relative permittivity of $\varepsilon = -3.1 + 2.5i$ at this wavelength.

It can be seen that the total electric energy density (depicted on the left of Fig. 2) strongly resembles the cylindrically symmetric field distributions predicted by Eq. (1) as well as numerical calculations via vectorial diffraction theory [17] for both cases (not shown). While the energy density distributions of the individual electric field components (right side of Fig. 2) show minor deviations from the expected symmetries given by Eq. (1), the resulting phase distributions (depicted as insets) exhibit the expected on-axis phase vortices with charge m and $m \pm 1$ for the transverse and longitudinal field components, respectively, in the case of the first-order Laguerre–Gaussian beam [Fig. 2(b)].

From this experimentally determined fully vectorial complex electric field distribution, we now trace the real-valued electric field vector on a circular path with radius $r = 150$ nm around the optical axis (shown in Fig. 2 as white or black dashed lines) for a fixed time t within an optical period T. For a fundamental Gaussian input beam $\mathrm{LG}_0^{\mathrm{circ}-}$, the electric field for $t = 0$ and $t = T/4$ traced along the closed circle features the topological structure of a twisted ribbon as depicted in Fig. 3(a). Dark and light blue arrows correspond to the two times indicated above. When following the trace in a ccw direction, the electric field vector rotates once in a cw manner around the trace, corresponding to a topological charge or twist index of the ribbon of -1 [15]. This index can also be inferred from the projection of the electric field vector onto the transverse plane, as shown in Fig. 3(a). To verify the experimentally obtained twist index, we additionally calculated the focal field distribution of a $\mathrm{LG}_0^{\mathrm{circ}-}$ beam with the same parameters used in Fig. 3(a) using vectorial diffraction theory [17], resulting in the twisted ribbon shown in Fig. 3(b). The excellent agreement of the experimentally determined and numerically calculated topological structures confirms their robustness against aberrations and experimental noise. Furthermore, our results show that such intriguing structures are

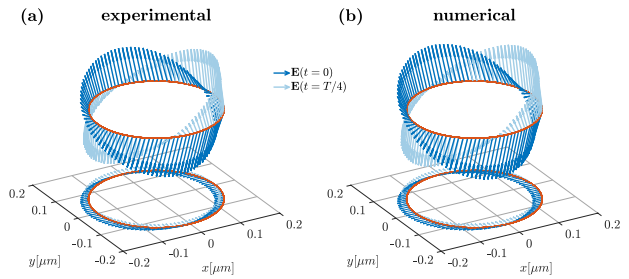

Fig. 3. 3D vector distributions of the instantaneous electric field vector in the focal plane of a tightly focused $\mathbf{LG_0^{circ-}}$ beam as well as its projection onto the transverse plane, traced on a ring of radius $r = 150$ nm at two different time moments of the optical period T, $t = 0$ and $t = T/4$. (a) The experimentally reconstructed 3D electric field ribbon with twist index -1, and (b) its numerically calculated counterpart for the same conditions as in (a) highlight the clockwise rotation of the electric field vector when tracing the circular path counterclockwise around the optical axis and show the very good correspondence between experiment and numerical calculation (see Visualization 1).

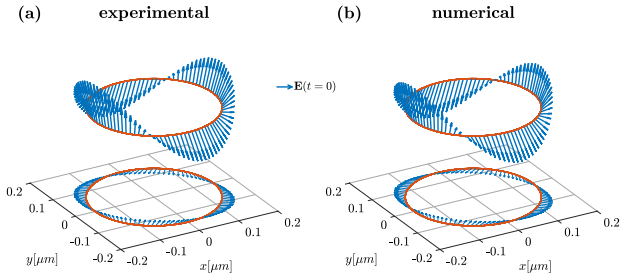

Fig. 4. 3D vector distributions of the instantaneous electric field vector in the focal plane of a tightly focused $\mathbf{LG}_1^{\mathbf{circ+}}$ beam as well as its projection onto the transverse plane, traced on a ring of radius $r = 150$ nm at a time $t = 0$ of the optical period T. (a) The experimentally reconstructed 3D electric field ribbon with twist index 2, and its numerically calculated counterpart for the same conditions as in (a) arise from the counterclockwise rotation of the electric field vector when tracing the circular path counterclockwise around the optical axis (see Visualization 2).

even present in the most fundamental and widely used light beams such as a circularly polarized fundamental Gaussian beam.

Comparing the resulting twisted ribbons for both time steps $t = 0$ and $t = T/4$ (light and dark blue arrows in Fig. 3), we can also follow the instantaneous rotation of the topological structure upon time evolution, confirming the analytically expected rotation at the optical frequency ω for the shown case of $m = 0$ (see also Visualization 1).

To verify the analytically determined twist index for higher-order light beams and probe a "pure" twisted ribbon around a dark spot of the electric field, we also plot the corresponding data for a Laguerre–Gaussian beam $\mathrm{LG}_1^{\mathrm{circ+}}$ [see Fig. 2(b)]. The resulting twisted ribbon with twist index 2 is depicted in Fig. 4(a) and agrees very well with the numerically determined twisted ribbon [Fig. 4(b)]. Here, a single optical cycle will lead to a rotation of the twisted ribbon topology by only 180° when traced around the optical axis (see Visualization 2), confirming the inverse relation between the rotation frequency of the focal field and its total AM.

In conclusion, we have analytically predicted and experimentally and numerically observed twisted ribbons formed by the time-instantaneous electric field vector *per se* with the number of full twists depending on the total AM of the underlying tightly focused light beam, $m \pm 1$, spinning in time around the optical axis at a $1/(m \pm 1)$ fraction of the optical frequency. Our findings show that beside the distribution of polarization (ellipse) and phase, the electromagnetic field itself can also feature an interesting topological structure. We envision that the underlying robustness of these entities might allow for novel concepts in shaping coherent multi-particle light–matter states such as hybrid polaritons.

Funding. Nederlandse Organisatie voor Wetenschappelijk Onderzoek; FP7 Ideas: European Research Council (340438); Russian Foundation for Basic Research (20-07-00505).

Acknowledgment. T. B., P. B., and G. L. thank S. Orlov for the initial theoretical implementation of the employed field reconstruction algorithm.

Disclosures. The authors declare no conflicts of interest.

REFERENCES

1. K. Y. Bliokh, F. J. Rodríguez-Fortuño, F. Nori, and A. V. Zayats, Nat. Photonics **9**, 796 (2015).
2. A. Aiello, P. Banzer, M. Neugebauer, and G. Leuchs, Nat. Photonics **9**, 789 (2015).
3. J. Leach, M. R. Dennis, J. Courtial, and M. J. Padgett, New J. Phys. **7**, 55 (2005).
4. H. Larocque, D. Sugic, D. Mortimer, A. J. Taylor, R. Fickler, R. W. Boyd, M. R. Dennis, and E. Karimi, Nat. Phys. **14**, 1079 (2018).
5. I. Freund, Opt. Commun. **249**, 7 (2005).
6. I. Freund, Opt. Lett. **35**, 148 (2010).
7. T. Bauer, P. Banzer, E. Karimi, S. Orlov, A. Rubano, L. Marrucci, E. Santamato, R. W. Boyd, and G. Leuchs, Science **347**, 964 (2015).
8. T. Bauer, M. Neugebauer, G. Leuchs, and P. Banzer, Phys. Rev. Lett. **117**, 013601 (2016).
9. M. Eberler, S. Quabis, R. Dorn, and G. Leuchs, Proc. SPIE **4777**, 362 (2002).
10. E. J. Galvez, I. Dutta, K. Beach, J. J. Zeosky, J. A. Jones, and B. Khajavi, Sci. Rep. **7**, 13653 (2017).
11. T. Bauer, P. Banzer, F. Bouchard, S. Orlov, L. Marrucci, E. Santamato, R. W. Boyd, E. Karimi, and G. Leuchs, New J. Phys **21**, 053020 (2019).
12. I. Freund, Opt. Lett. **39**, 727 (2014).
13. I. Freund, Opt. Lett. **27**, 1640 (2002).
14. E. Pisanty, G. J. Machado, V. Vicuña-Hernández, A. Picón, A. Celi, J. P. Torres, and M. Lewenstein, Nat. Photonics **13**, 569 (2019).
15. I. Freund, Opt. Lett. **36**, 4506 (2011).
16. T. Bauer, S. Orlov, U. Peschel, P. Banzer, and G. Leuchs, Nat. Photonics **8**, 23 (2014).
17. B. Richards and E. Wolf, Proc. R. Soc. London A **253**, 358 (1959).
18. S. Khonina and I. Golub, J. Opt. Soc. Am. A **29**, 1470 (2012).
19. S. Khonina and I. Golub, J. Opt. Soc. Am. A **33**, 1948 (2016).
20. S. Khonina, A. V. Ustinov, and S. G. Volotovsky, Opt. Laser Technol. **60**, 99 (2014).
21. S. Khonina and I. Golub, J. Opt. Soc. Am. B **36**, 2087 (2019).
22. J. Durnin, J. J. Miceli, and J. H. Eberly, Phys. Rev. Lett. **58**, 1499 (1987).
23. G. T. Di Francia, Nuovo Cimento **9**, 426 (1952).
24. Y. Zhao, J. S. Edgar, G. D. M. Jeffries, D. McGloin, and D. T. Chiu, Phys. Rev. Lett. **99**, 073901 (2007).
25. S. Khonina and I. Golub, Opt. Lett. **41**, 1605 (2016).
26. L. Marrucci, C. Manzo, and D. Paparo, Appl. Phys. Lett. **88**, 221102 (2006).
27. E. Karimi, G. Zito, B. Piccirillo, L. Marrucci, and E. Santamato, Opt. Lett. **32**, 3053 (2007).